The Spatial Distribution and Temperature of Mercury's Potassium Exosphere

Patrick Lierle[1][2], Carl Schmidt[2], Jeffrey Baumgardner[2], Luke Moore[2], Tom Bida[3], Ryan Swindle[4]

[2]*Boston University, Boston, MA, USA*

[3]*Lowell Observatory, Flagstaff, USA*

[4]*Air Force Research Labs, Kihei, HI, USA*

Abstract:

Aside from the well-studied sodium doublet, the potassium D lines are the only optical emissions in Mercury's exosphere that are amply bright to contrast with the dayside disk. Measurements of the K exosphere are limited compared to Na, but the K regolith abundance is better constrained, so new insights may help to understand surface–exosphere coupling. We use imaging spectroscopy to map the K brightness over Mercury's evening hemisphere, which shows an enhancement at low to midlatitudes, well equatorward of the Na peak. Both Na and K are brighter in the south, but the ratio between northern and southern hemisphere K emission appears less symmetric than that of Na. The disk-averaged Na/K column density ratio is between 70 and 130. During the same night, the dayside emission was mapped, we used a high-resolution spectrograph to attempt to resolve the Na and K line widths on the nightside. Forward-modeling the alkaline line profiles with hyperfine structure gives Na D1 and D2 line widths of $1114 \pm 50$ K and $1211 \pm 45$ K, respectively. D2 may appear hotter solely because its higher opacity adds preferentially to the profile wings. The K line width is surprisingly cold and cannot be easily distinguished from the instrumental line width, even at $R = 137{,}500$. Line widths roughly constrain K gas between the surface temperature and 1000 K, making it the coldest metallic constituent of Mercury's exosphere. Although Na and K are chemical analogs and often assumed to have similar properties, the results herein illustrate quite different characteristics between these elements in Mercury's exosphere.

---

[1] Corresponding author plierle@bu.edu
[2] Center for Space Physics, Boston University, 725 Commonwealth Ave, Boston MA 02215, USA
[3] Lowell Observatory, 1400 W Mars Hill Rd, Flagstaff, AZ 86001, USA
[4] Air Force Research Laboratory, 550 Lipoa Pkwy # 100, Kihei, HI 96753

## 1. Background:

Ground-based observations of Mercury have detected the presence of sodium, potassium (Potter & Morgan 1985, 1986), calcium (Bida et al. 2000), aluminum, and iron (Bida & Killen 2017) in its surface boundary exosphere. MESSENGER confirmed these and additionally detected magnesium (McClintock et al. 2009) and manganese (Vervack et al. 2016), but it failed to confirm the oxygen detection by Mariner 10, the probe responsible for the first detection of atomic hydrogen and helium (Broadfoot et al. 1976). Sodium and potassium are the only two of these constituents that are bright enough to observe against Mercury's bright disk, while also producing emission lines that are available to ground-based observers. The ability to easily observe sunlight scattered by these elements allows them to act as tracers for source processes feeding Mercury's exosphere. The source processes sustaining Mercury's exosphere include photon-stimulated desorption, thermal desorption, ion sputtering, and micrometeorite impacts. Their relative roles have long been debated, but each process has predictable characteristics in temperature and spatial distribution, and so sodium and potassium measurements over the disk can help disentangle the complex system of sources and sinks.

The existing body of research on K is substantially smaller than that of Na. Potassium is a more challenging observation from the ground, and K emissions at 7665 and 7699 Å fall redward of the MESSENGER UltraViolet and Visual Spectrometer spectral range. Moreover, Earth's molecular oxygen typically blocks the brighter of the two K-D lines, except under certain Doppler shifts. In principle, as chemical analogs with similar photoionization and radiation pressure effects, Na and K should exhibit similar properties like temperature and spatial distribution. Models have treated the two species together (Smyth & Marconi 1995). While properties of the sodium exosphere are much better constrained than those of potassium, the opposite case is true of Mercury's surface mineralogy. Na in the regolith appears to be concentrated at high latitudes, at least in the northern hemisphere, but the distribution with longitude is unknown (Peplowski et al. 2014). K soil concentrations have been mapped in the northern hemisphere and appear anticorrelated with the maximum annual surface temperature, i.e., concentrated at high latitudes and cold-pole longitudes (Peplowski et al. 2012).

The first detection of exospheric potassium was made by Potter & Morgan (1986), who reported $10^9$ K atoms $cm^{-2}$ and an Na/K ratio of 80. Potter et al. (2002) refined Mercury's average Na/K to 100 and pointed out that this ratio well exceeds that of nearly all other solar system bodies, particularly the Moon, where the 4.4–6 ratio is approximately stoichiometric with the soil. Noting that other direct source/sink differences could not explain this difference, they proposed that Mercury's anomalously high Na/K could result from differences in ion behavior, whereby Na+ is more efficiently recycled back into the surface and K+ is preferentially lost into the solar wind owing to its larger gyroradius. Hunten & Sprague (1997) found an even higher Na/K ratio of 400, and Doressoundiram et al. (2010) reported a spatially dependent Na/K ratio between 80 and 400. Killen et al. (2010) generated a 0.5" spatial resolution full-disk map of the Na/K ratio, which showed a latitude dependence also present in the Doressoundiram et al. (2010) results, but peaked near 100 at high latitudes, with equatorial values of around 30. Such differences are not necessarily in conflict since Na ejection rates from Mercury's surface are episodic in nature, due to both space weather (Orsini et al. 2018) and stochastic meteoroid bombardment (Cassidy et al. 2021), and it is unknown whether the K ejection varies proportionally. Leblanc & Doressoundiram (2011)

modeled the potassium exosphere and concluded that differences in transport, loss, and desorption efficiencies can explain the spatial variation in Na/K. When these differences are considered, they asserted that Mercury's high Na/K ratio may in fact be consistent with initial solar or meteoric abundance.

Polar enhancements in the sodium exosphere are a prominent feature generally attributed to ion precipitation though the magnetospheric cusps (Potter & Morgan 1990). Due to the northward offset of Mercury's dipolar magnetic field, more surface area is exposed to open magnetic field lines in the southern hemisphere. A global maximum Na density is often reported above this region (e.g., Baumgardner et al. 2008; Leblanc et al. 2008; Mangano et al. 2013; Schmidt et al. 2020), but, like the magnetosphere, the sodium distribution is dynamic (e.g., Leblanc et al. 2009; Mangano et al. 2015). Thus far, polar enhancements collocated with ion precipitation seem to be a phenomenon that is unique to Na. Such features have not been reported in the other exospheric constituents, and potassium measurements are currently too limited to offer a robust constraint.

Another feature apparently unique to sodium is the exospheric enhancement above the cold-pole longitudes (90° and 270°), where Mercury's orbital eccentricity and 3:2 spin–orbit resonance produce a cooler surface (Cassidy et al. 2016; Milillo et al. 2021). The longitudinal distribution of Na mineralogy is unknown, but potassium indeed shows higher soil concentrations at these two longitudes (Peplowski et al. 2012). This suggests that the surface–exosphere coupling of both alkali species is thermally dependent and that this dependence shares some similarity between them. However, the temperature of Mercury's potassium exosphere is an important consideration that remains observationally unconstrained.

## 2. Observations:

Table 1 lists a coordinated observing campaign from two facilities during Mercury's 2018 December elongation at a true anomaly angle of 76°–81°. Imaging spectroscopy data were obtained with the R ∼ 95,000 Rapid Imaging Planetary Spectrograph (RIPS), located at the 3.7 m Advanced Electro Optical System (AEOS) telescope (Haleakala, Hawaii). RIPS captured potassium D1 emissions above Mercury's dayside at solar elongation with integration times ranging from 5 to 200 s. The 5 s integrations enabled even progression of the slit while scanning across Mercury's disk with adaptive optics, while long exposures served as a backup in case K emission was not measurable in the shorter frames. During the same run, RIPS also targeted the sodium D lines, with results from high-cadence imaging reported in Schmidt et al. (2020). AEOS locked onto a fixed image of the disk using adaptive optics, and the slit was manually scanned across the 7" planetary disk by pivoting RIPS on a stage. Wavelength-dependent refraction is an important consideration at high air mass. Since narrowband images were captured at sodium wavelengths, a ∼2" on-sky translation was calculated at this air mass and applied between potassium spectra and the accompanying narrowband images of Mercury.

Table 1: December 2018 observations of Mercury by RIPS and EXPRES.

| UT Start Time | Target | Airmass | $N_{frames}$ | Integration (s) | Pointing |
|---|---|---|---|---|---|
| *RIPS* | | | | | |
| 2018-12-12 15:51:11-16:25:29 | K | 7.75-4.00 | 500 | 5 | Dayside (Figure 5) |

| 2018-12-12 15:36:14-15:47:11 | Na | 12.80-8.69 | 700 | 1 | Dayside |
|---|---|---|---|---|---|
| 2018-12-13 16:12:07-16:20:45 | K | 4.91-4.28 | 5 | 100 | Dayside (Figure 7) |
| 2018-12-13 16:22:49-16:29:59 | K | 4.15-3.76 | 3 | 200 | Dayside (Figure 7) |
| 2018-12-13 15:38:51-15:49:23 | Na | 11.46-8.11 | 700 | 1 | Dayside |
| *EXPRES* | | | | | |
| 2018-12-13 13:24:58-13:26:38 | Na & K | 7.07-6.78 | 1 | 100 | 1 (Figure 1) |
| 2018-12-13 13:28:31-14:07:27 | Na & K | 6.58-3.81 | 4 | 500 | 2-5 (Figure 1) |
| 2018-12-13 14:08:53-14:13:53 | Na & K | 3.72-3.54 | 1 | 300 | 6 (Figure 1) |

Hours earlier, across the Pacific Ocean, EXtreme PREcision Spectrometer (EXPRES) captured high-resolution spectra from the 4.3 m Lowell Discovery Telescope in Arizona. EXPRES was designed for exoplanet radial velocity measurements (Jurgenson et al. 2016; Brewer et al. 2020; Cabot et al. 2021). Over the course of six integrations, EXPRES recorded sodium and potassium on Mercury's nightside, just behind the terminator. EXPRES pointing at the nightside served to better contrast the exosphere against the bright scattered continuum. Compared to RIPS's long slit, EXPRES employs a 0.9" circular aperture mounted in a triangular housing, as is seen in Figure 1, along with the aperture locations for each of the six frames. EXPRES data are not used to determine any spatial information herein, and the duration of twilight observations did not permit spatial scanning of the small aperture. The broad free spectral range of EXPRES captures sodium and potassium concurrently, and an atmospheric dispersion corrector is incorporated into the instrument's design. Observations from EXPRES overlap with those from RIPS on 1 day, 2018 December 13, and consist of integration times in the range of 100–500 s.
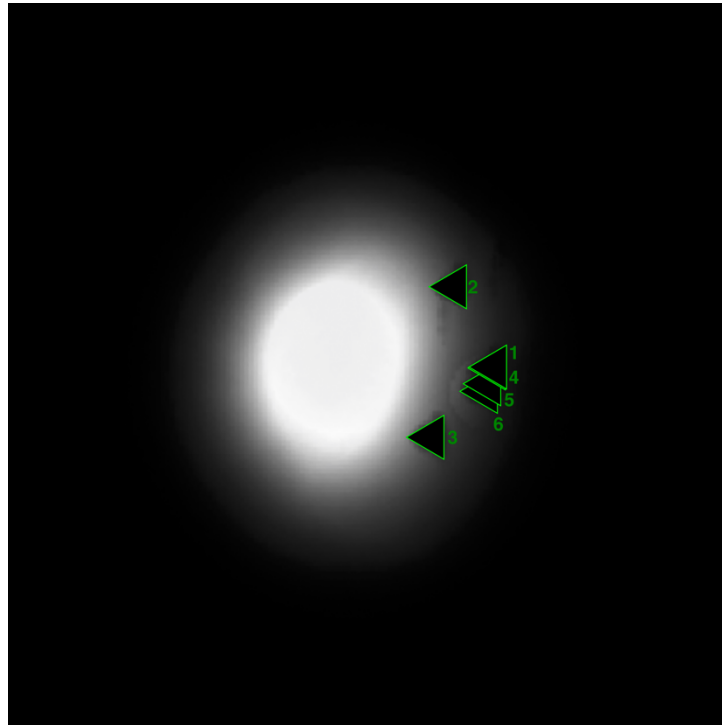


*Figure 1: Locations of the EXPRES aperture for each of the six frames acquired on 13 December 2018. This shows fast tip-tilt slit-viewing camera frames co-aligned over all measurements with a plate scale of 0.16"/px. Pointing is concentrated just off-disk beyond the evening terminator.*

An example raw RIPS frame is shown in Figure 2. RIPS simultaneously records a narrowband image and a high-resolution spectrum (spectral range of <30 Å) onto a single Andor iXon 1024 × 1024 EMCCD using mirrored slit jaws. The imaging channel, with a plate scale of 0.045" pixel$^{-1}$ at AEOS, provides both spatial registration of the slit aperture on the planet's disk and a reference for the instantaneous atmospheric seeing, enabling a calibration for absolute brightness. The spectral channel is a dispersed mirror image of the light passing through the slit aperture, magnified by 12%.
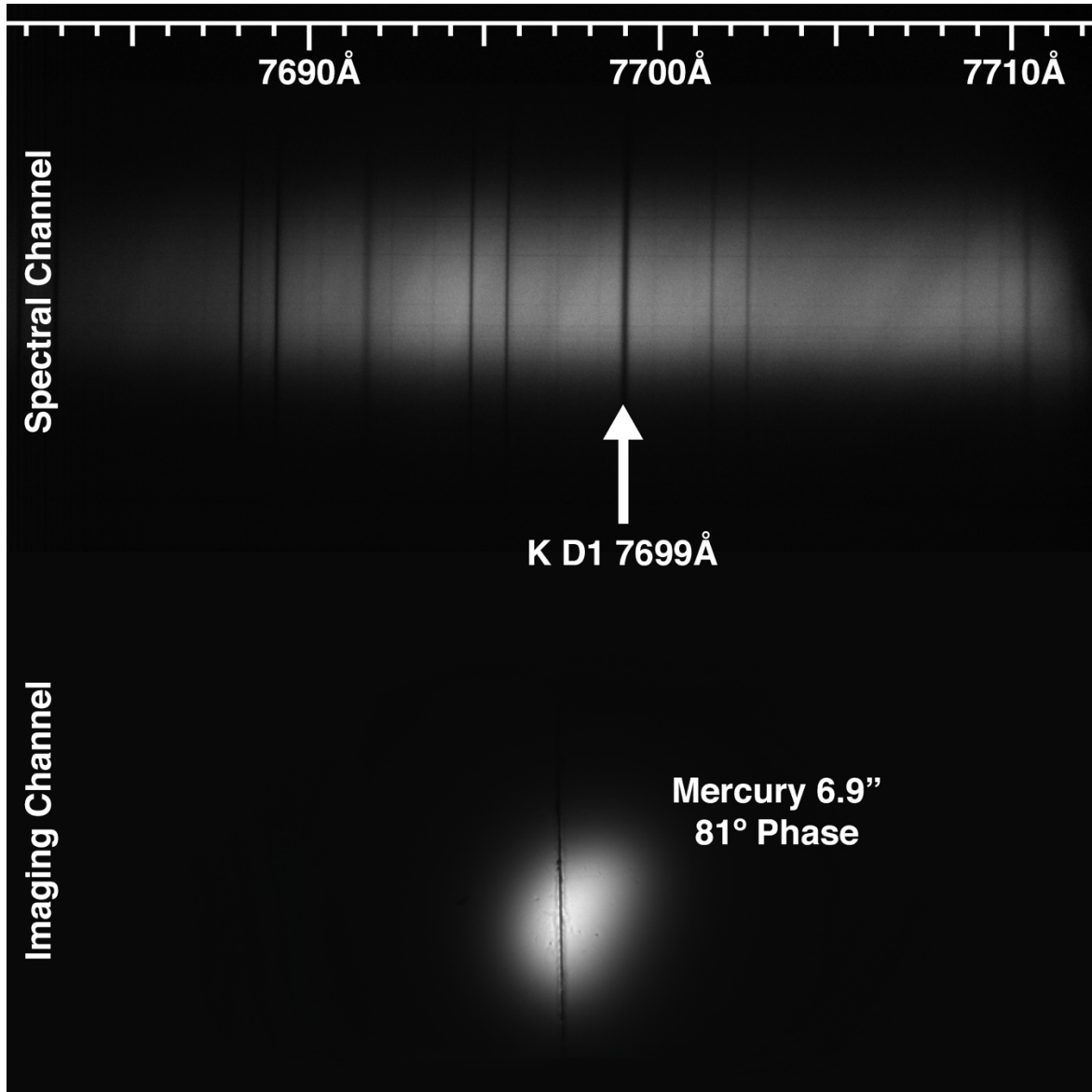


*Figure 2: A raw 200s RIPS integration of Mercury at 81° phase angle with the K 7699Å solar absorption line nearly centered. This is a single CCD image with the spectra recorded on the top half of the detector and the narrowband image on the bottom half. The spectral channel has been multiplied by 15 artificially here to improve visibility.*

### 3. Photometric Modeling and Analysis with RIPS:

Analysis of the RIPS data set employs a photometric model of Mercury's surface reflectance. This treatment uses Hapke's basic formulation (Hapke 2012; Equation (12.55)) combined with parameters determined from the MESSENGER Mercury Dual Imaging System (MDIS) data set by Domingue et al. (2016). The photometric model is matched to the RIPS instrumental plate scale and observational geometry at AEOS, interpolating the Hapke parameters at the MDIS filter bands to a featureless continuum wavelength of 7697 Å. This provides a surface reflectance determination for each pixel on the RIPS imaging channel. Combining this model with solar spectral irradiance, adjusted for Mercury–Sun geometry and blurred for atmospheric seeing, yields a theoretical model for the continuum brightness at each pixel at a given wavelength—the reference needed for determining the empirical brightness of the potassium exosphere.

RIPS data are first prepared by performing corrections for flattening the field, bias, and dark signal. The two detector channels, spectral and imaging, are then separated for independent processing. Beginning with the imaging channel, each frame is interpolated over the slit, to generate a "slitless" disk. Cross-correlation between a blurred Hapke image and the slitless imaging channel data first determines the plane-of-sky rotation angle and then the spatial registration of Mercury. These parameters are applied to spatially align each of the images and spectra. An estimate for atmospheric seeing in each frame is then determined by cross-correlation. Figure 3 shows a narrowband image captured by RIPS, along with the corresponding photometric model before and after blurring for atmospheric seeing.
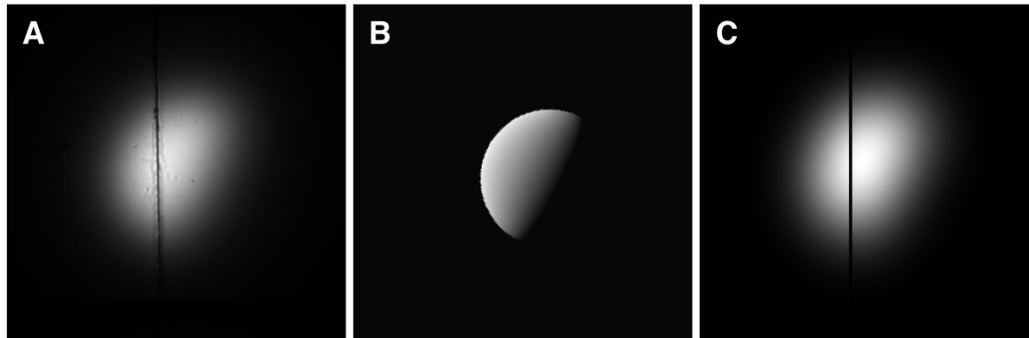


*Figure 3: A: A raw narrowband image of Mercury reflected by RIPS's mirrored slit jaws. B: A photometric model of Mercury's surface reflectance matched to the observation geometry. C: The photometric model, blurred to match the atmospheric seeing, superimposed with a re-creation of RIPS's slit.*

Next, the potassium signal is extracted from the spectral channel of each frame. Pixel-to-pixel noise can exceed the K emission signal, and so spatial binning is needed. The data are binned both along the slit and across multiple frames with adjacent pointing. We found that constructing five bins of 1.9" along the slit produces measurable potassium emission in each bin for a 200 s equivalent spectrum. A solar spectrum is convolved with a Gaussian kernel to match to the native RIPS resolution. This spectrum is fit to the solar-reflected potassium well and surrounding

continuum and subtracted. The resulting residual contains solely exospheric emission, which is summed over line width.

To flux-calibrate this potassium signal, a 1 Å band of featureless continuum at 7697 Å is summed and processed alongside the potassium emission. Combining this with the blurred 7697 Å photometric model, we obtain a sensitivity factor in (Rayleigh*s)/DN, which is multiplied by the K signal to generate an absolute brightness. It is then straightforward to recover column density from the "g-value" excitation rate by solar photons, using Mercury's heliocentric distance and velocity at the time of measurement (see Chamberlain & Hunten 1987). We applied a g-value of 61.151 photons atom$^{-1}$ s$^{-1}$ to K D1, 21.112 photons atom$^{-1}$ s$^{-1}$ to Na D1, and 56.398 photons atom$^{-1}$ s$^{-1}$ to Na D2.

## 4. Linewidth Modeling and Temperature Estimation with EXPRES:

A forward model of the K D1 emission line is employed to estimate temperature from the EXPRES data, and the Na D1 and D2 lines serve as a valuable reference for this technique. The sodium gas temperature at Mercury has been independently determined in two ways: atmospheric scale height, which gives ~1200 K at optically thin altitudes (Cassidy et al. 2015), and line width modeling, previous estimates of which have suggested that the Na gas is 600–700 K above surface temperature (Killen et al. 1999). The technique we apply follows Brown & Yung (1976, Equations (13) and (15)). The absorption coefficient per atom is used to generate Doppler profiles for each hyperfine line, which are then summed to generate D1 and D2 line profiles (note that a factor of 22 inside of the exponential term was omitted in Brown & Yung's originally published Equation (15)). Figure 4 shows the resulting profile at several temperatures. While this treatment incorporates potassium D-line hyperfine structure components from Welty et al. (1994, Table 4), we find that hyperfine components can be neglected at the temperatures of Mercury's dayside and K D1 emission is well represented by a single Gaussian. Na hyperfine structure is more broadly separated (~23 mÅ for D1), and so hyperfine structure in the line profile becomes important.
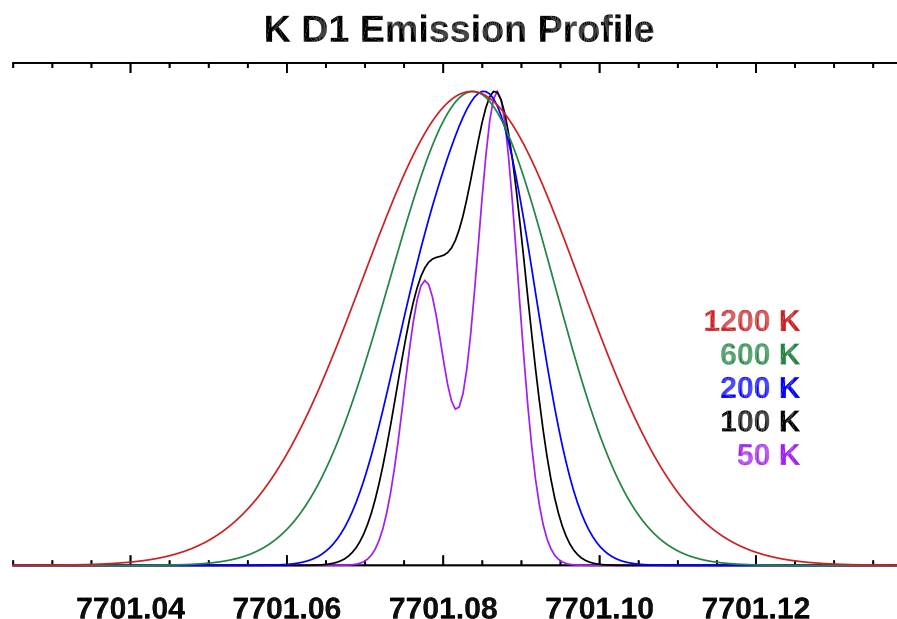
EXPRES has high resolving power (R = 137,500) and the advantage of a stable and narrow instrumental line spread function (FWHM ~61mÅ at 7698Å). The spectra were processed through the data pipeline detailed in Petersburg et al. (2020). All six EXPRES integrations from 13 December 2018 are co-added to form the single spectrum in the present analysis. As with RIPS analysis, spectral regions surrounding the three emission features, Na D1, D2, and K D1, are individually fit with a solar spectrum,[1] which is subtracted to generate a residual containing only exospheric emission. Next, the forward-model for each line is input into a fitting routine which varies its temperature and amplitude while also convolving it with a Gaussian kernel of the instrumental linewidth. This instrumental linewidth is larger at the potassium D1 line than at the sodium doublet, and so different kernels are used depending on which feature is being fit. The fitting routine performs a least-squares fit on each of the three emission features, returning an estimated best-fit temperature for each.
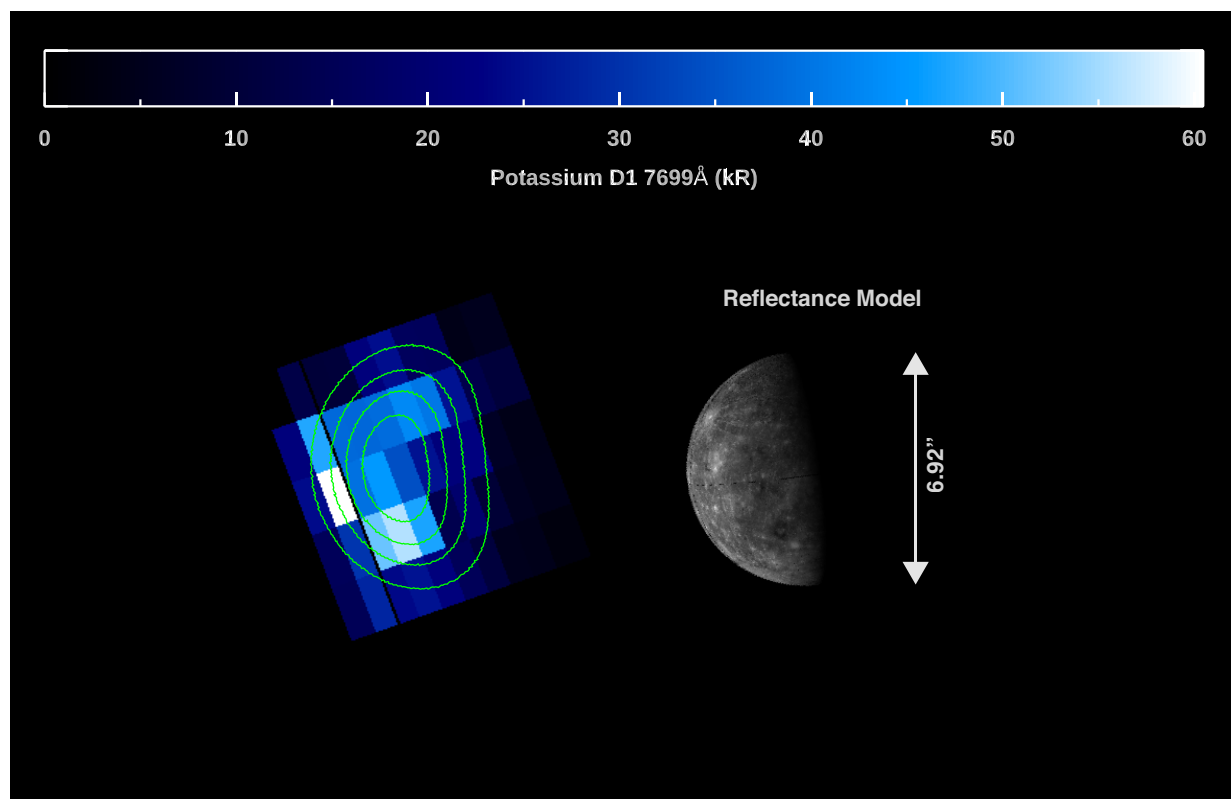
## 5. Spatial Distribution of Potassium:



*Figure 5: Exospheric potassium brightness from the RIPS 5s integration full-disk scans on December 12, 2018. North is up and this faces Mercury's evening hemisphere. Pictured at right is an unconvolved photometric reflectance model of Mercury at the time and geometry of*

---

[1] http://kurucz.harvard.edu/sun.html

*observation, which has been overlaid with surface topography. The green contours are constructed from the photometric model after it has been convolved to match the mean atmospheric seeing.*

A full-disk map of potassium across Mercury in shown in Figure 5, as constructed from the 500 frames of 5 s each captured by RIPS on 2018 December 12. A reference image of Mercury is constructed by overlaying the photometric model with surface topography and shown to scale. The spectra were combined into 10 bins across the disk and 5 bins along the slit to attain adequate signal-to-noise ratio (average on-disk S/N ~ 5). The peak potassium brightness is 61 kR, corresponding to $1.0 \times 10^9$ atoms cm$^{-2}$. Local densities may be higher if the emitting region is unresolved. Unlike the surface concentration, the exospheric K distribution is enhanced at low to midlatitudes. K emission is particularly strong in the southern hemisphere and near the subsolar point. Ion precipitation through the southern cusp covers a broader area of Mercury's surface, but the K emission here is concentrated equatorward of Na peaks resolved in concurrent RIPS sodium data by Schmidt et al. (2020), and well equatorward of the magnetic cusps. The north/south ratio is more pronounced than is typical of sodium, though these ratios have been observed to vary (Schmidt et al. 2020 report a range from 0.7 to about 1.03 N/S), presumably with the solar wind and interplanetary magnetic field conditions at Mercury (Mangano et al. 2015).
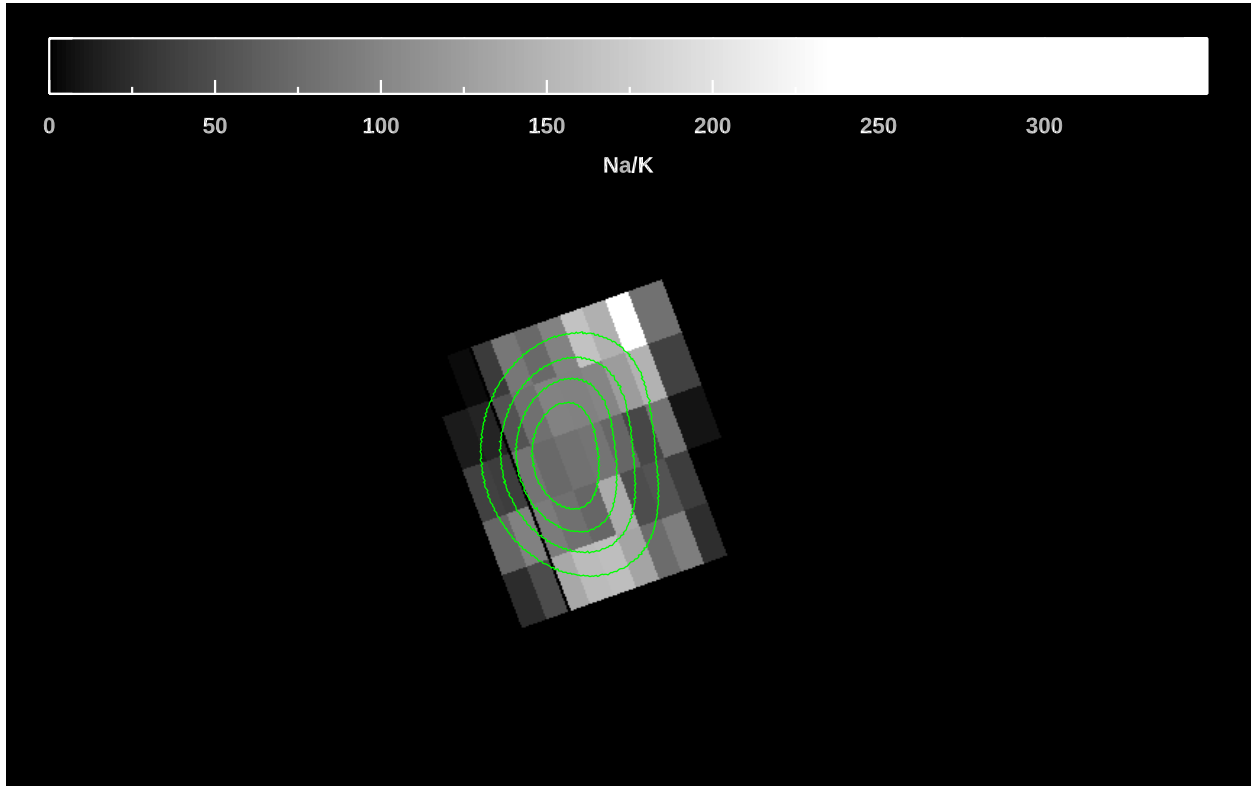


*Figure 6: Full-disk Na/K column density ratio generated by binning same-day RIPS sodium measurements to match the spatial dimensions of the potassium results from December 12, 2018.*

Figure 6 shows a full-disk map of the sodium-to-potassium column ratio from 2018 December 12, wherein sodium emissions in Schmidt et al. (2020) have been spatially binned to

match the K results in Figure 5. The disk-averaged Na/K ratio is ~70, with the ratio highest at and just behind Mercury's poles. This map of the ratio reflects the presence of strong sodium enhancements at the poles in both hemispheres and potassium enhancements located at lower latitudes. The brightest pixel above Mercury's north pole is likely a result of noise-dominated potassium signal, but polar Na/K is reliably in the range of 90–150. Near the subsolar point, Na/K drops to ~50.
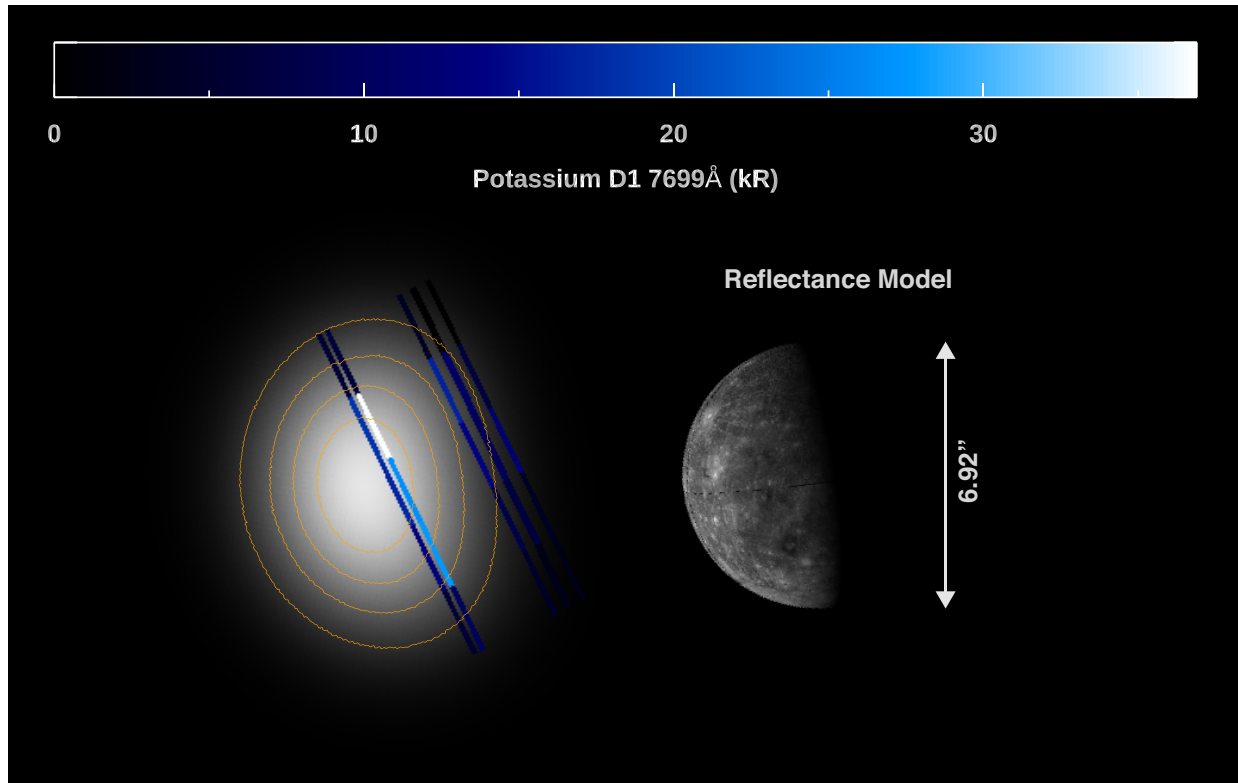


*Figure 7: Potassium brightness in the five slit positions covered by RIPS during its 100-200s integrations on December 13, 2018. Pictured at right is an unconvolved photometric reflectance model of Mercury at the time and geometry of observation, which has been overlaid with surface topography. The orange contours are constructed from the photometric model after it has been convolved match the mean atmospheric seeing.*

Figure 7 shows the potassium emission from 2018 December 13. Five discrete slit positions across Mercury's disk are superimposed over a photometric model blurred to the average seeing of the eight individual frames. Frames taken at the same slit position are averaged, resulting in five unique slit positions. A reference image of Mercury is constructed by overlaying the photometric model with surface topography and shown to scale. Note that the Caloris Basin, a surface feature that Sprague et al. (1990) connected to K exosphere enhancements, is on the nightside in this viewing geometry. D1 emission in this partial map peaks at 37 kR ($6.0 \times 10^8$ cm$^{-2}$), and a local Na/K ratio of 106 is obtained here from the simultaneous Na map in Schmidt et al. (2020). The Na/K column ratio in Figure 8 again peaks at high latitudes, and the Na/K ratio averaged over all 25 spatial bins is ~130.
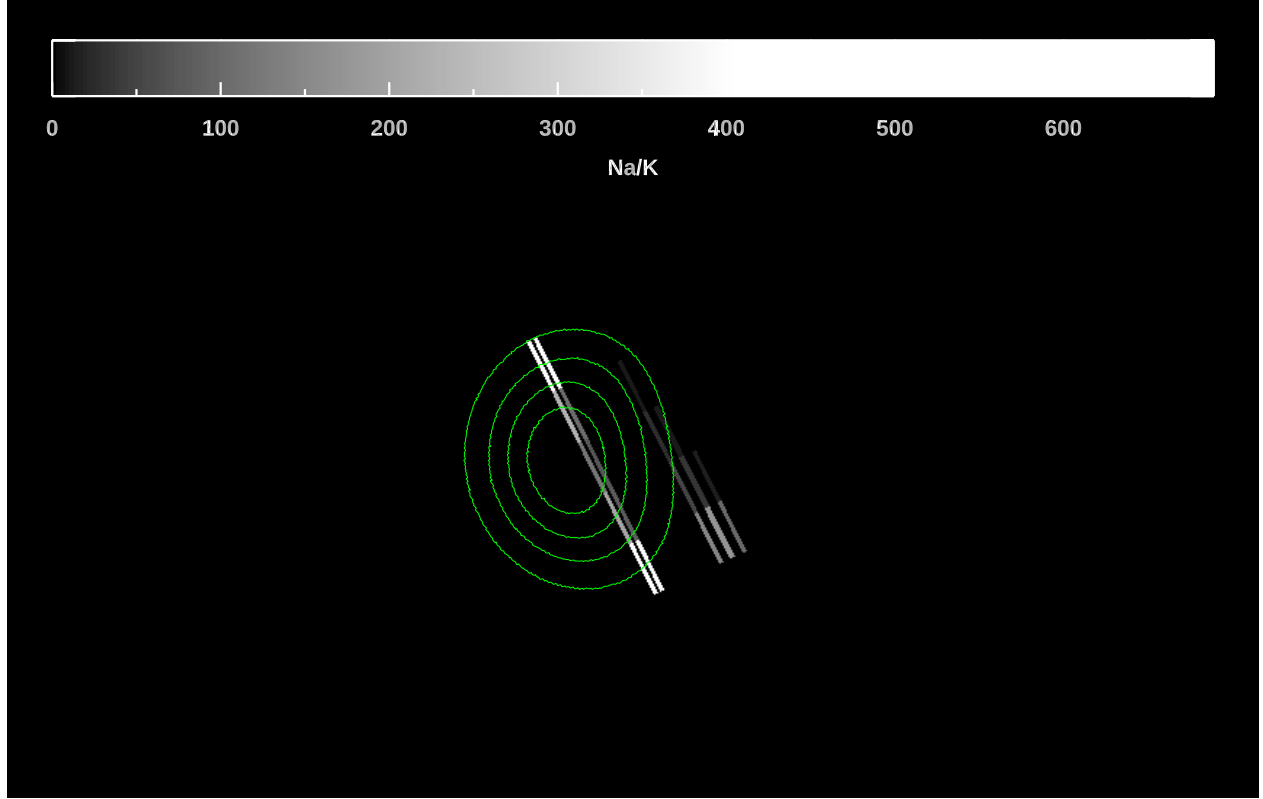
*Figure 8: The Na/K ratio map corresponding to RIPS sodium and potassium brightness measurements from December 13, 2018.*

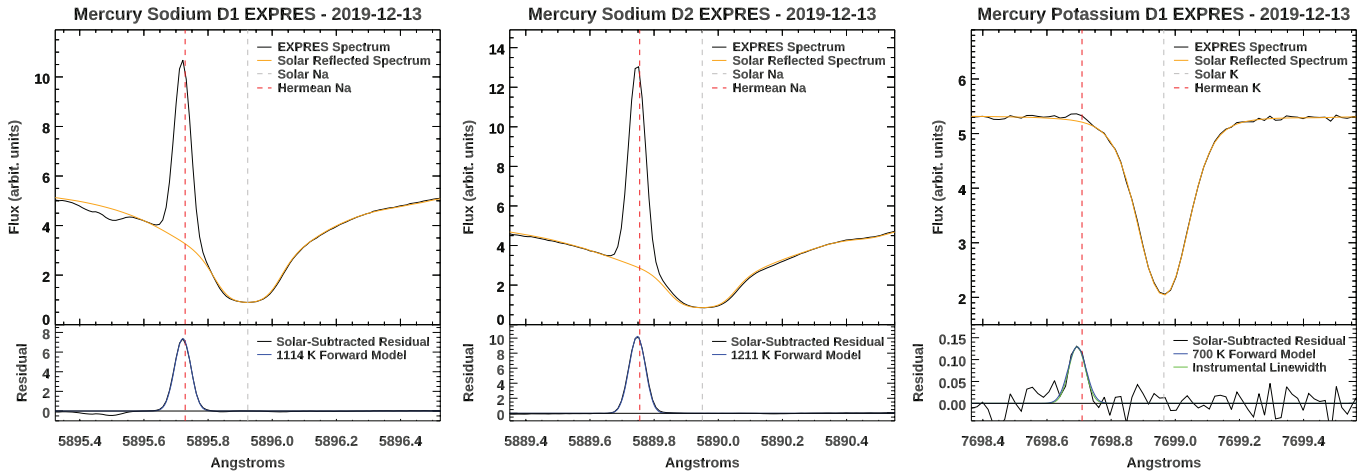## 6. Linewidth Measurements



*Figure 9: Continuum removal and fitting to estimate a linewidth temperature for the sodium doublet and potassium D1. The grey and red dashed lines indicate the central wavelength of the solar well and the expected wavelength of emission from Mercury, respectively.*

Figure 9 shows the sodium doublet and potassium D1 line emissions before and after subtraction of the bright solar continuum. These spectra are uncorrected for telluric features, and Earth's

absorption lines (e.g., at 5895.5 Å) are excluded from the fitting region. The offset between emission lines and their expected position given Mercury's Doppler shifts is not an artifact and is discussed in Section 7. The forward models best fit to the data are overplotted in each lower panel, resulting in the following temperature estimates: $1114 \pm 50$ K and $1211 \pm 45$ K for Na D1 (S/N $\sim$ 43) and D2 (S/N $\sim$ 73), respectively. Both are in close agreement with the $\sim$1200 K MESSENGER estimate based on atmospheric scale height (Cassidy et al. 2015). D2 perhaps exhibits a broader line width owing to opacity effects, in which the line core saturates while the wings grow, making it appear hotter (Killen 2006). Na D1 is a more direct temperature proxy, as it has half the opacity of D2; on this date, its line center optical depth is $\sim$0.4 within the peak column of $1.3 \times 10^{11}$ cm$^{-2}$.
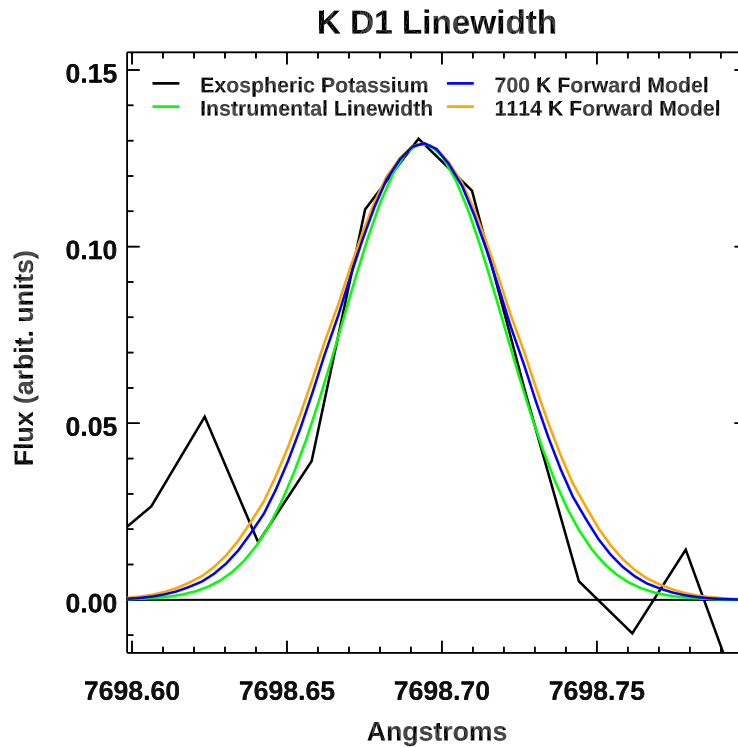


*Figure 10: The potassium D1 line, as compared with the instrumental line spread function, a 700K model characteristic of the surface temperature at the subsolar point, and an 1114K model, the temperature of sodium D1.*

Analysis of the K D1 line indicates that potassium is colder than sodium, so much so that it is difficult to distinguish from the instrumental line width, even at a resolution of $R = 137,500$. The algorithm fit to the Na lines fails to converge at K D1 because the line profile is evidently narrower than the instrumental line width. This is a nonphysical result and likely a consequence of the noise levels in the line profile (S/N $\sim$ 6), but it still offers some insight. Given that the fit only worsens with increasing temperature above 0 K and that there is an absence of cooling mechanisms in Mercury's exosphere, we hypothesize that potassium may be near the subsolar surface temperature. A forward model of 700 K, characteristic of the subsolar surface (Hunten &

Sprague 1997), is overplotted for comparison with the residual, as is the 1114 K temperature of sodium D1. Differences between these curves are subtle but nonetheless indicate that the characteristic energy of K is lower than Na. Consequently, this implies that K is the coldest metallic constituent of Mercury's exosphere. The measurement here is challenging and hence limited in accuracy, but this result is not inconsistent with K atoms that are in thermal equilibrium with the surface temperature.

All three emission features in Figure 9 fall just blueward of their expected position as determined by the instantaneous Mercury–Sun Doppler shifts. This is not a consequence of the radiation pressure considering the 82° phase angle with the tail orientation in redshift. Leblanc et al. (2009) have reported a similarly globally negative Doppler shift for sodium, the implication being that, due to ionization and atmospheric escape, more gas is being ejected from Mercury than is returning to its surface. The shifts are radially negative because atoms are ejected from the hemisphere facing the observer. Leblanc et al. (2009) measured global shifts around −0.9 km s$^{-1}$ for Na D2, while the D2 shift in our Figure 9 is determined to be −0.46 km s$^{-1}$. Considering that EXPRES was pointed on the nightside, there may be a small redshift component from radiation pressure, which could explain the lesser magnitude compared to Leblanc et al. (2009). Potassium D1 has a shift of −0.57 km s$^{-1}$, which we attribute to the shorter K ionization lifetime and the higher K radiation acceleration relative to Na, both of which remove atoms that would otherwise fall back to the surface. This mechanism is our best guess at why all three emissions are blueshifted, but it is an open area of investigation, and we invite other ideas. Lastly, although the EXPRES data are not calibrated for absolute flux, the Na/K ratio can still also be estimated from these data by comparing their relative brightness and $g$-values. This produces an Na/K ratio of ∼120 on the nightside, marginally higher than that determined in Figures 6 and 8.

## 7. Discussion:

Combining results from RIPS and EXPRES, we have generated a range of values for the average Na/K ratio. On December 12, the disk-averaged Na/K ratio is found to be ∼70. The following night, the average Na/K ratio for a smaller region of the disk is ∼130. Lastly, the Na/K ratio just behind the terminator, as determined by EXPRES data over several nights in December, is ∼120. This set of values lies within the range of disk-averaged ratios reported in Potter et al. (2002) (Na/K ∼ 34–142). It is at the lower end of the range of spatial variations in the ratio that Doressoundiram et al. (2010) reported (Na/K ∼ 80–400) while being slightly greater than those hemisphere-averaged values reported by Killen et al. (2010; Na/K ∼ 36–74) across the planet's dayside. The disk-averaged K column density obtained from Figure 5 results in an associated disk-averaged brightness for the K 404 nm doublet (Killen et al. 2009) of 50 Rayleigh. Vervack et al. (2016) did not detect this strong of an emission above 200 km, but at a temperature of 700 K, this is a distance of five potassium scale heights, plausibly accounting for the discrepancy.

The full-disk maps of K emission in Figure 5 confirm the prior finding of Potter & Morgan (1997) and Killen et al. (2010) that the potassium exosphere is concentrated predominately in Mercury's southern hemisphere, although the column density they derived is several times higher (Potter & Morgan: (2.1–4.6) × 10$^9$ atoms cm$^{-2}$). Potter et al. (2002) did not spatially resolve the disk, but Doressoundiram et al. (2010) and Killen et al. (2010) both measured highest Na/K ratios

at the poles, in concordance with findings herein. Together this affirms that K is likely concentrated equatorward of Na in the Mercury exosphere. Such is the expectation if K were liberated by thermal desorption or photodesorption near the hot subsolar region and cold-trapped elsewhere, as Peplowski et al. (2014) proposed to explain the K soil concentration. Based on laboratory measurements, ballistic K atoms are also less likely to bounce across the hot dayside compared to Na (Yakshinskiy & Madey 2005), and so fewer atoms pushed by radiation pressure from sources near the subsolar point should reach the poles and terminator. Still, Na yields from the surface are clearly sensitive to plasma bombardment since the Na exosphere appears dynamic and frequently concentrated near the cusp footprints. Evidently, this is not so for processes yielding potassium.

The narrow line widths measured here, as seen in Figure 10, point to thermal desorption or photodesorption as the dominant mechanism for potassium release, as sputtered or meteoroid-vaporized K would appear much hotter. The treatment here assumes a thermally distributed population, but this assumption is not necessarily valid in a collisionless exosphere. Yakshinskiy & Madey have conducted a series of laboratory experiments on desorption induced by electron transfer in ionically bonded solid alkalis, which is the underlying mechanism for photodesorption. They found that Na and K atoms were both ejected with a characteristic energy of ~0.1 eV. Yet, as seen in Figure 11, neither energy distribution is discernibly Maxwellian, and the K distribution around 0.1 eV is quite narrow, lacking the high-energy tail of the Na population (Yakshinskiy & Madey 2003). Such a distribution would produce a stronger potassium line core relative to the wings, but it cannot explain widths anywhere narrower than the instrumental line width in Figure 10. Nonthermal line profiles are beyond our scope of modeling at present, but based on their experiments, photodesorbed K should exhibit less Doppler broadening than Na.
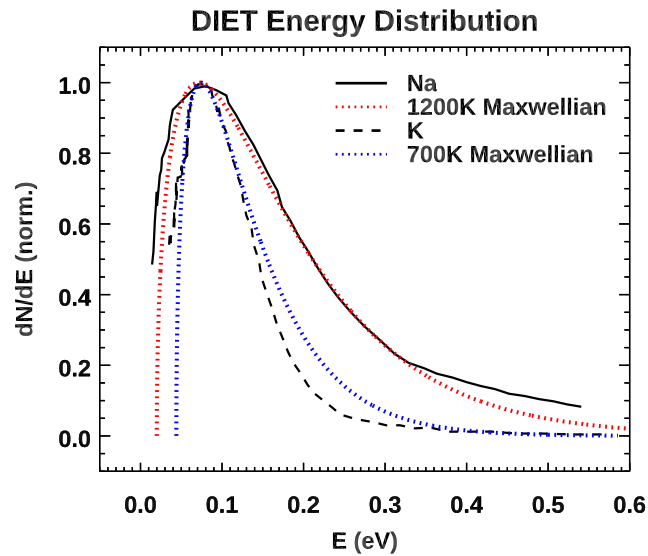


**DIET Energy Distribution**

*Figure 11: Laboratory energy distributions of Na and K desorbed from a SiO₂ surface (Yakshinskiy & Madey, 2003). 1D Maxwell-Boltzmann distributions are overlaid at 1200K and 700K. Neither species is*

*discernably Maxwellian, but Na exhibits a high-energy*
*tail which is absent from the narrower, less-thermal K.*

The PHEBUS instrument aboard BepiColombo (Quémerais et al., 2020) features a dedicated channel for the potassium doublet near 404 nm. These lines were not detected by the MESSENGER spacecraft, however, Vervack et al. (2016) discovered that a manganese triplet at 403nm does emit within this passband. Therefore, we anticipate ground-based measurements of the brighter potassium lines will be useful to disentangle potassium from manganese in the upcoming PHEBUS measurements.

## 8. Conclusions:

We find that Mercury's Na and K exospheres exhibit significant differences in both their spatial distribution and temperature, well beyond those expected given their chemical similarity. Potassium emission is characterized by low to midlatitude enhancement, while sodium abundance peaks at higher latitudes, proximal to the magnetic cusps. Potassium emission also exhibits a greater north–south asymmetry than sodium, with the strongest emission in the south. The peak potassium brightness is found to be 60 kR, with an associated column density of $1.0 \times 10^9$ atoms $cm^{-2}$. Disk-averaged Na/K ratio estimates, determined from same-day observations of the two species, range from 70 to 130, with the ratio greatest at high latitudes and just behind Mercury's poles on the nightside, where sodium column density is much higher than that of potassium. Additionally, K line widths indicate a lower gas temperature, making potassium the coldest metallic constituent of Mercury's exosphere at <1000 K. While noise levels preclude a more precise constraint on the potassium temperature, these results are consistent with potassium being thermalized to the hot dayside surface. By spending a full night on potassium (less than 1 hr due to geometry) and forgoing comparative sodium measurements, it is expected that a future study could produce a higher-resolution potassium map to further characterize the K exosphere.

**References:**

Baumgardner, J., Wilson, J., & Mendillo, M. 2008, GeoRL, 35, L03201

Bida, T. A., & Killen, R. M. 2017, Icar, 289, 227

Bida, T. A., Killen, R. M., & Morgan, T. H. 2000, Natur, 404, 159

Brewer, J. M., Fischer, D. A., Blackman, R. T., et al. 2020, AJ, 160, 67

Broadfoot, A. L., Shemansky, D. E., & Kumar, S. 1976, GeoRL, 3, 577

Brown, R. A., & Yung, Y. L. 1976, Jupiter, Studies of the Interior, Atmosphere, Magnetosphere
        and Satellites (Tucson, AZ: Univ. Arizona Press), 1102

Cabot, S. H. C., Roettenbacher, R. M., Henry, G. W., et al. 2021, AJ, 161, 26

Cassidy, T. A., McClintock, W. E., Killen, R. M., et al. 2016, GeoRL, 43, 11,121

Cassidy, T. A., Merkel, A. W., Burger, M. H., et al. 2015, Icar, 248, 547

Cassidy, T. A., Schmidt, C. A., Merkel, A. W., Jasinski, J. M., & Burger, M. H. 2021, PSJ, 2,
        175

Chamberlain, J. W., & Hunten, D. M. 1987, Theory of Planetary Atmospheres: An Introduction
        to their Physics and Chemistry, Vol. 36 (2nd ed.; Orlando, FL: Academic Press Inc.)

Domingue, D. L., Denevi, B. W., Murchie, S. L., & Hash, C. D. 2016, Icar, 268, 172

Doressoundiram, A., Leblanc, F., Foellmi, C., et al. 2010, Icar, 207, 1

Hapke, B. 2012, Icar, 221, 1079

Hunten, D. M., & Sprague, A. L. 1997, AdSpR, 19, 1551

Jurgenson, C., Fischer, D., McCracken, T., et al. 2016, Proc. SPIE, 9908, 99086T

Killen, R. M. 2006, PASP, 118, 1344

Killen, R. M., Potter, A., Fitzsimmons, A., & Morgan, T. H. 1999, P&SS, 47, 1449

Killen, R. M., Potter, A. E., Vervack, R. J., et al. 2010, Icar, 209, 75

Killen, R. M., Shemansky, D., & Mouawad, N. 2009, ApJS, 181, 351

Leblanc, F., & Doressoundiram, A. 2011, Icar, 211, 10

Leblanc, F., Doressoundiram, A., Schneider, N., et al. 2009, GeoRL, 36, L07201

Leblanc, F., Doressoundiram, A., Schneider, N., et al. 2008, GeoRL, 35, L18204

Mangano, V., Massetti, S., Milillo, A., et al. 2013, P&SS, 82, 1

Mangano, V., Massetti, S., Milillo, A., et al. 2015, P&SS, 115, 102

McClintock, W. E., Vervack, R. J., Bradley, E. T., et al. 2009, Sci, 324, 610

Milillo, A., Mangano, V., Massetti, S., et al. 2021, Icar, 355, 114179

Orsini, S., Mangano, V., Milillo, A., et al. 2018, NatSR, 8, 928

Peplowski, P. N., Evans, L. G., Stockstill-Cahill, K. R., et al. 2014, Icar, 228, 86

Peplowski, P. N., Lawrence, D. J., Rhodes, E. A., et al. 2012, JGRE, 117, E00L04

Petersburg, R. R., Joel Ong, J. M., Zhao, L. L., et al. 2020, AJ, 159, 187

Potter, A. E., & Morgan, T. H. 1985, Sci, 229, 651

Potter, A. E., Anderson, C. M., Killen, R. M., & Morgan, T. H. 2002, JGRE, 107, 5040

Potter, A. E., & Morgan, T. H. 1986, Icar, 67, 336

Potter, A. E., & Morgan, T. H. 1997, P&SS, 45, 95

Potter, A. E., & Morgan, T. H. 1990, Sci, 248, 835

Quémerais, E., Chaufray, J. Y., Koutroumpa, D., et al. 2020, SSRv, 216, 67

Schmidt, C. A., Baumgardner, J., Moore, L., et al. 2020, PSJ, 1, 4

Smyth, W. H., & Marconi, M. L. 1995, ApJ, 441, 839

Sprague, A. L., Kozlowski, R. W. H., & Hunten, D. M. 1990, Sci, 249, 1140

Vervack, R. J., Killen, R. M., McClintock, W. E., et al. 2016, GeoRL, 43, 11545

Welty, D. E., Hobbs, L. M., & Kulkarni, V. P. 1994, ApJ, 436, 152

Yakshinskiy, B. V., & Madey, T. E. 2003, SurSc, 528, 54

Yakshinskiy, B. V., & Madey, T. E. 2005, SurSc, 593, 202